Delft University of Technology

The role of silicon in carbon partitioning processes in martensite/austenite microstructures

Kim Lee, B.N.; Sietsma, J.; Santofimia Navarro, Maria

DOI
[10.1016/j.matdes.2017.04.080](https://doi.org/10.1016/j.matdes.2017.04.080)

Publication date
2017

Document Version
Final published version

Published in
Materials & Design

Citation (APA)
Kim Lee, B. N., Sietsma, J., & Santofimia Navarro, M. (2017). The role of silicon in carbon partitioning processes in martensite/austenite microstructures. *Materials & Design*, *127*, 336-345. https://doi.org/10.1016/j.matdes.2017.04.080
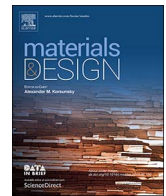
Important note
To cite this publication, please use the final published version (if applicable).
Please check the document version above.

Copyright
Other than for strictly personal use, it is not permitted to download, forward or distribute the text or part of it, without the consent of the author(s) and/or copyright holder(s), unless the work is under an open content license such as Creative Commons.

Takedown policy
Please contact us and provide details if you believe this document breaches copyrights.
We will remove access to the work immediately and investigate your claim.

This work is downloaded from Delft University of Technology.
For technical reasons the number of authors shown on this cover page is limited to a maximum of 10.

The role of silicon in carbon partitioning processes in martensite/austenite microstructures

B. Kim[*], J. Sietsma, M.J. Santofimia

Department of Materials Science and Engineering, Delft University of Technology, Mekelweg 2, Delft 2628 CD, The Netherlands

ABSTRACT

Understanding carbon redistribution in steels is crucial in developing advanced high strength steels. For instance, Quenching & Partitioning (Q & P) processes rely on the partitioning of carbon from martensite into austenite, where at the end of the heat treatment the carbon-enriched austenite shows higher stability at room temperature. Recent literature gives increasing evidence of carbide precipitation occurring during partitioning despite the addition of silicon, conventionally thought to suppress carbide precipitation. The aim of the present study is to gain insight into carbon-competing processes by applying a series of Q & P heat treatments, with particular focus on the partitioning stage, where the role of silicon in the stability of austenite is evaluated. Various characterisation techniques are combined in order to unveil the microstructural changes. While carbide precipitation does appear to occur in the presence of silicon, it is found that silicon plays an active role in the stabilisation of the austenite during the partitioning reaction.

GRAPHICAL ABSTRACT
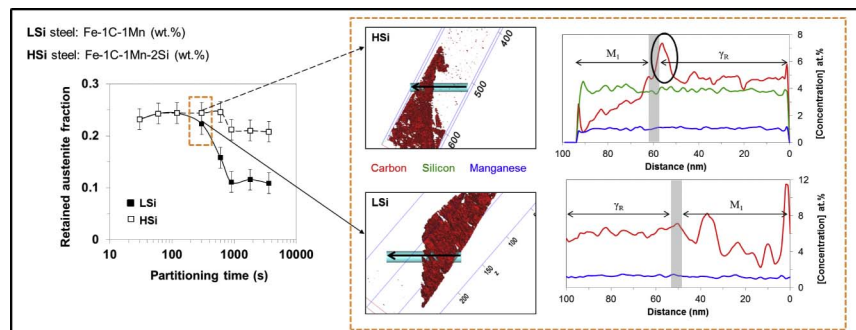
1. Introduction

Advanced high strength steels typically consist of complex microstructures that are optimised by both heat treatment and alloying composition. Understanding the redistribution of carbon within the microstructure during processing is fundamental in designing new steels, but still remains a challenge due to the various carbon-competing processes that occur throughout the heat treatment. In the case of Quenching & Partitioning (Q & P) steels, heat treatments are designed

such that carbon partitions from martensite into austenite, where at the end of the heat treatment the carbon-enriched austenite shows higher stability at room temperature. The Q & P heat treatment typically consists of austenitising and quenching to a temperature between the martensitic start temperature and room temperature, in order to obtain a desired fraction of martensite in the microstructure. The steel is then reheated to a higher temperature, where carbon partitioning from martensite into austenite occurs. At the end of the partitioning stage, the sample is quenched to room temperature. During this second

* Corresponding author.
E-mail address: B.N.KimLee@tudelft.nl (B. Kim).

quench, the austenite that is not sufficiently enriched in carbon transforms into martensite.

The typical microstructure developed during a Q & P heat treatment consists of

- M_1– this is the martensite that forms during the first quench, where the fraction of M_1 depends on the quenching temperature (QT) and becomes carbon-depleted and tempered during the partitioning stage;
- γ_R– this is the austenite that is retained at the end of the heat treatment after the sample is cooled to room temperature (RT); and
- M_2– this is the fresh martensite that forms during the second quench, having a higher carbon content than M_1 since it forms from carbon-enriched (although insufficiently) austenite.

These are the notations that will be used throughout the present study to denominate the different products forming throughout the heat treatment.

In the Q & P design, carbide precipitation must be suppressed in order to allow maximum carbon partitioning from martensite into austenite. In this aspect, Q & P steels are typically alloyed with silicon [1,2]. Nevertheless, recent literature gives evidence of more complex interactions involving carbon: (i) there is increasing evidence of carbide precipitation occurring during partitioning [3–5], and (ii) recent literature also indicates that carbon solubility in ferrite when in equilibrium in austenite is higher than predicted using conventional thermodynamic databases [6,7]. Both phenomena are relevant to the Q & P process as they reduce the amount of carbon available to partition into austenite, hence the stability of the austenite at the end of the thermal cycle becomes affected. The present study focuses on point (i) carbide precipitation, where the role of silicon will be investigated.

Carbide precipitation during martensite tempering is not surprising, especially if considering the paraequilibrium conditions in which carbides form by inheriting the matrix composition including the silicon content [8–10]. Hence the precise role of silicon in Q & P steels is questioned. Furthermore, during the partitioning stage there is also the possibility of austenite decomposing into bainite [5]. In a different context, in recent work on bearing steels technology by Sourmail and Millot-Méheux [11] it was shown that the addition of silicon enhances the thermal stability of γ_R against decomposition into ferritic products during tempering. Therefore, it is the aim of the current study to gain insight into the role of silicon in carbon-partitioning processes and its influence on the stability of austenite by applying a series of Q & P style heat treatments, with particular focus on the partitioning stage. Quantitative characterisation techniques such as dilatometry, X-ray diffraction (XRD) and atom probe tomography (APT) are combined in order to unveil the role of silicon in carbon partitioning processes.

From the studies it is observed that carbide precipitation occurs even in the presence of silicon. On the other hand, silicon is seen to enhance austenite stability and inhibit the decomposition of austenite during partitioning. Furthermore, it is also observed that martensite formation is accompanied by transformation strain in austenite, affecting austenite's lattice parameter, which may give an unreliable carbon content estimation in austenite.

2. Experimental procedure

Two model alloys have been selected for the purpose of this study, where the chemical compositions are shown in Table 1. A relatively high carbon content (1 wt% C) was chosen for the following reasons: (i) owing to the high carbon content a relatively low M_s is expected, thus minimising the effect of autotempering during the quenching process which would affect the carbon content in M_1 before the partitioning stage is reached, and (ii) the supersaturation of the carbon in ferrite solid solution is likely to give rise to tetragonality of the martensite forming upon the final quench, hence M_1 and M_2 can be distinguished by X-ray diffraction (XRD). The as-received material was in the form of hot-rolled plate of 6 mm thickness.

The heat treatments applied were Q & P style heat treatments, shown in Fig. 1. In the first set of heat treatments, Fig. 1 (a), a series of different quenching temperatures were applied for fixed austenitisation and partitioning conditions. In the second set, Fig. 1 (b), the effect of partitioning time was studied for two quenching temperatures. The heat treatments were carried out using a Bähr DIL 805 A/D dilatometer, where cylindrical samples of 3.5 mm diameter and 10 mm length were obtained from the middle of the rolled plate, parallel to the rolling direction. The heating rate used was 5 °C/s and all quenching processes were done using helium gas. The measured cooling rate from the thermocouples was ~ 150 °C/s between 1000 °C and M_s. First, experiments were carried out in order to determine the martensitic start temperature, M_s. Using the offset method [12], M_s of alloys LSi and HSi were determined to be 151 ± 1 °C and 140 ± 6 °C, respectively.

In order to determine the volume fraction of γ_R, M_1 and M_2, X-ray diffraction experiments were performed using a Bruker type D8-Advance diffractometer equipped with a Bruker Vantec Position Sensitive Detector (PSD). Co Kα radiation was used, for scans in the 35–140° 2θ range. The obtained diffractograms were analysed by Rietveld refinement using the MAUD software [13].

In order to study local variations in carbon concentration and other alloying elements, one particular condition from alloys LSi and HSi was examined by atom probe tomography (APT) using a local electrode atom probe (LEAP 4000X HR) at Eindhoven University of Technology. The microtips were prepared by FIB (dual beam FEI Nova600i NanoLab), where prior EBSD measurements were made in order to specify the regions of interest (ZEISS Ultra 55 equipped with HIKARI EBSD camera with TSL software). APT analyses were performed using laser pulse mode, where measurements were taken at 20 K, 30 pJ laser energy and 200 kHz pulse rate. The reconstructions were performed using the IVAS 3.6.8 software, with settings of delocalisation 2.5 nm and voxel size 0.7 nm. Peak decomposition was carried out using the algorithm provided in the IVAS software.

3. Results and discussion

3.1. Dilatometry

The dilatometry results obtained during the final quench from the set of heat treatments listed in Fig. 1 (a) are summarised in Fig. 2. As seen in Fig. 2 (a), a full quench in the dilatometer from 1000 °C to room temperature leads to an incomplete martensitic transformation in both alloys. In Fig. 2 (b) it is observed that the formation of M_2 in the final cooling is dependent on QT. No M_2 formation is detected in dilatometry for the QT50. The trend is clearly seen in Fig. 2 (c), where M_s of M_2 is seen to decrease linearly with a decrease in QT. Following the Q & P line of thought, a lower QT produces higher fractions of M_1, increasing the amount of carbon available to partition from the super-saturated ferrite into austenite. Hence, under the same partitioning conditions, a higher M_1 fraction will likely result in higher carbon-enrichment in austenite at the end of the partitioning stage. Since the M_s decreases with increasing carbon contents [14], a decrease in M_s upon final cooling is an indication of higher carbon content in austenite prior quenching.
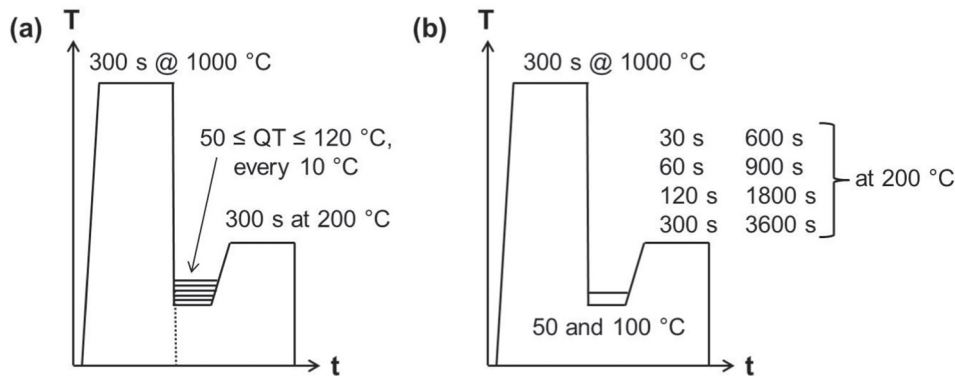
Table 1
Measured chemical composition of steels in wt% (in at.%), where Fe is to balance, and the measured M_s determined by dilatometry.

	C	Mn	Si	Al	M_s (°C)
Alloy LSi	1.00 (4.49)	1.08 (1.06)	0.01 (0.01)	0.01 (0.02)	151 ± 1
Alloy HSi	0.98 (4.40)	1.04 (1.02)	1.98 (3.80)	0.01 (0.02)	140 ± 6

Fig. 1. Illustration of heat treatments applied to alloys LSi and HSi, where (a) the quenching temperature (QT) varies, and (b) the partitioning time varies after quenching to 50 °C and 100 °C.
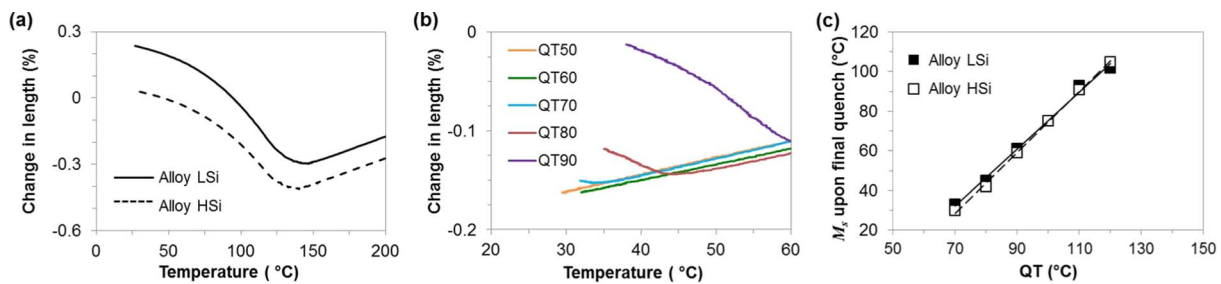

Fig. 2. (a) Dilatometry signal of martensite formation during full quench to RT. (b) Dilatometry signal of martensite formation during cooling to RT after quenching and partitioning steps (example shown for alloy HSi, except for conditions QT100–QT120). (c) Plot summarising the measured M_s temperature upon final quench for the heat treatments in Fig. 1 (a).
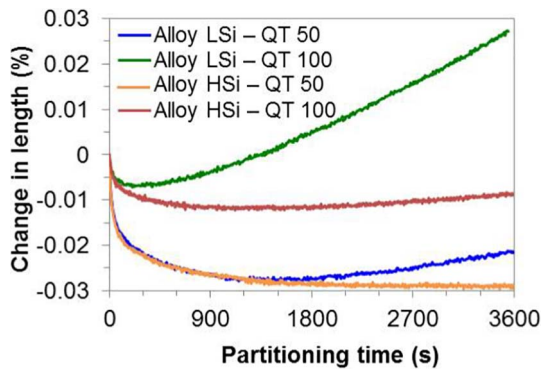
Fig. 3. Dilatation measured during partitioning for 3600 s.

From Fig. 2 (c), the same behaviour is seen to take place in both alloys LSi and HSi. However, as will become apparent later in this paper, the transformation strain in austenite could also play a role in stabilising the austenite phase.

Fig. 3 represents the change in length during the partitioning stage for the sample being partitioned for 3600 s, where time zero is taken as the point where the dilatometer reaches 200 °C. It is inferred that there are three processes that would lead to a volume change of the material in the dilatometer during the partitioning stage. The decomposition of austenite into ferrite will lead to an increase in atomic volume of iron, corresponding to an expansion in the dilatometer. On the other hand, carbon depletion within martensite as a result of carbon partitioning processes will lead to a reduction in the unit cell size, hence a contraction in dilatometry. Lastly, enrichment of carbon in austenite contributes to an expansion. Interpreting Fig. 3, it is deduced that for samples QT 50, the main process occurring in the first 1500 s is carbon depletion of martensite for both alloys LSi and HSi either by partitioning into austenite or into carbides. After the first 1500 s, decomposition of austenite becomes dominant in alloy LSi, whereas in alloy HSi, a plateau appears to have been reached.

For the QT 100 samples, alloy HSi shows an initial contraction, which reaches a plateau level around 900 s, and after 1800 s a gradual expansion is observed. As for alloy LSi, after an initial contraction, a
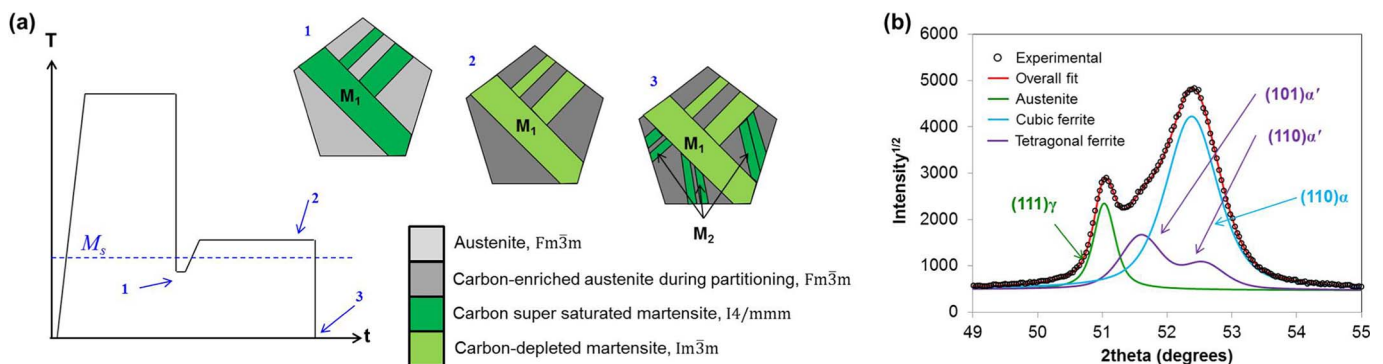

Fig. 4. (a) Diagram for distinguishing the different phases present in the sample after the Q & P heat treatment, and (b) example of the decomposition of ferrite and austenite peaks showing cubic ferrite (α), austenite (γ) and tetragonal ferrite (α').

Table 2
XRD analysis of the samples following full quench to room temperature.

Alloy	γ_R fraction	a_{γ_R} (nm)	c/a of martensite
LSi	0.21 ± 0.02	0.35975 ± 0.00001	1.043 ± 0.001
HSi	0.18 ± 0.02	0.35980 ± 0.00001	1.043 ± 0.001

large expansion is observed, hinting a faster austenite decomposition process in alloy LSi. Nevertheless, these interpretations are made based on the global dilatometry signal, where in reality the processes of carbon depletion of martensite, carbon enrichment in austenite and austenite decomposition occur simultaneously.

3.2. XRD

The samples processed according to Fig. 1 (b) were analysed using XRD. Consistent with the results in Section 3.1, no M_2 was observed in the XRD spectra for the QT 50 samples. On the other hand, for the QT 100 samples, which showed a dilatation of the sample during the final quench, the presence of tetragonal martensite was confirmed using XRD. For the QT 100 samples, in order to distinguish between γ_R, M_1 and M_2, the procedure outlined in Fig. 4 (a) is followed. It is assumed that during partitioning, M_1 becomes sufficiently carbon-depleted to render a cubic structure; the tetragonality observed at the end of the heat treatment is thus assumed only to be arising from M_2. The phases considered during Rietveld refinement were austenite (space group $Fm\bar{3}m$), cubic ferrite (space group $Im\bar{3}m$) and tetragonal ferrite (space group $I4/mmm$) for modelling γ_R, carbon-depleted martensite (α) and carbon-rich martensite (α'), respectively. An example of the fitting done showing the modelled decomposition into the $\{111\}_\gamma$ and $\{110\}_\alpha$ peaks is shown in Fig. 4 (b). Splitting of the ferrite peak is observed as a distinct shoulder in the martensite peak, where carbon-depleted martensite and carbon-rich martensite can be distinguished.

It is remarked that due to the small fractions of carbides and the limited resolution of the XRD equipment used in the present study, it was not possible to resolve carbide peaks. Therefore the carbide phases are omitted in the Rietveld refinement process, hence the fraction of austenite, tetragonal ferrite and cubic ferrite sum to unity. However, the fractions will become proportionally lower by the fraction of carbide present in the microstructure.

In principle, the fractions of carbon-depleted martensite (cubic α) and carbon-rich martensite (tetragonal α') are assumed to relate to the fractions of M_1 and M_2, respectively. However, this is no longer the case if austenite decomposition occurs during the partitioning stage. HajyAkbary et al. [5] showed that for some processing conditions, bainite formation from austenite in Q & P processes steels. Carbon was observed to partition from bainitic ferrite to austenite, which would lead to carbon depletion in bainitic ferrite. Hence in the current study, the ferrite product from austenite decomposition is considered to contribute to the cubic ferrite fraction, following the findings in [5].

XRD studies were also conducted on samples that have undergone direct quenching from 1000 °C to 25 °C. The fraction of γ_R, its lattice parameter and the tetragonality of the martensite are summarised in Table 2. The γ_R content in the as-quenched condition is relatively large, consistent with the incomplete martensitic transformation at room temperature, as seen in Fig. 2 (a). The carbon content in solid solution can be determined from the tetragonality of the martensite by

$$c/a = 1 + 0.045x_C^{\alpha'}, \tag{1}$$

where c and a are the lattice constants of the tetragonal ferrite, and $x_C^{\alpha'}$ is the weight concentration of carbon (wt%) in solid solution [15]. Both alloys show a tetragonality of 1.043 which corresponds to ∼ 0.96 wt% carbon. This closely matches the measured bulk carbon composition of the alloy. The carbon concentration in austenite, $x_C^{\gamma_R}$, is thought to be similar, or slightly higher, than this value.

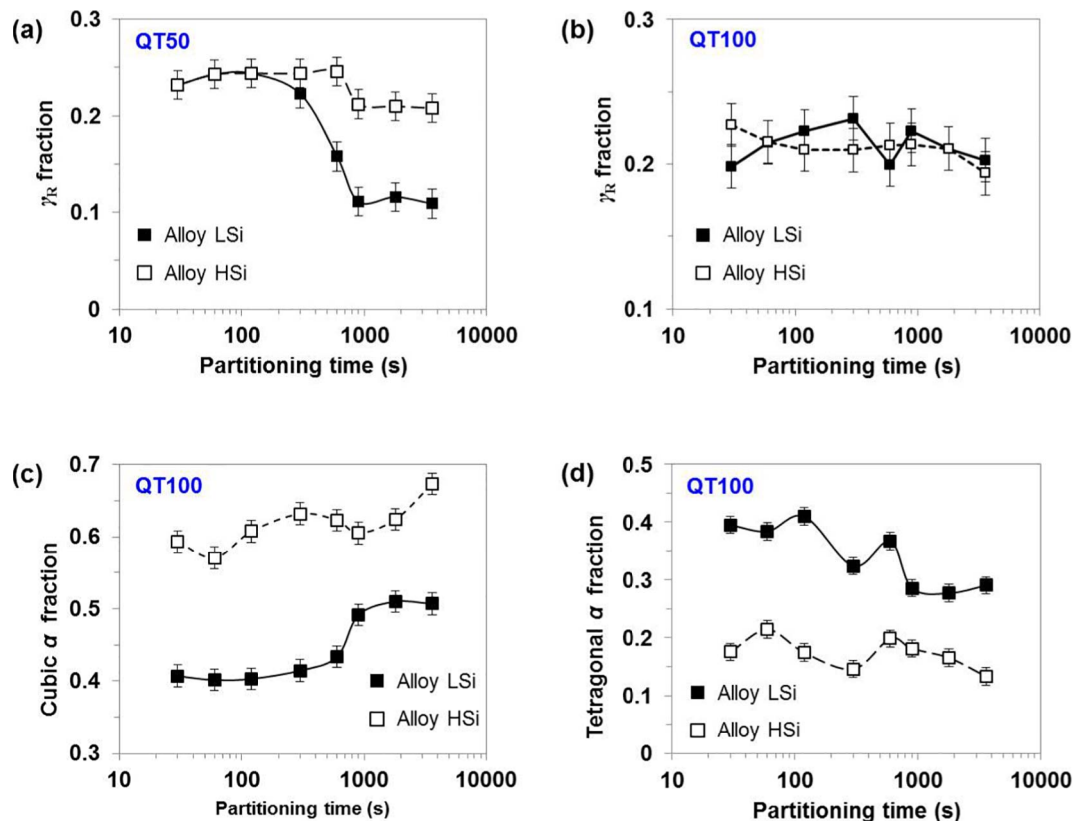The results from XRD for the heat treatments in Fig. 1 (b) are

Fig. 5. Measured fractions of (a) γ_R in QT 50 samples, (b) γ_R in QT 100 samples, (c) M_1 in QT 100 samples, and (d) M_2 in QT 100 samples. The fractions have been determined by XRD.
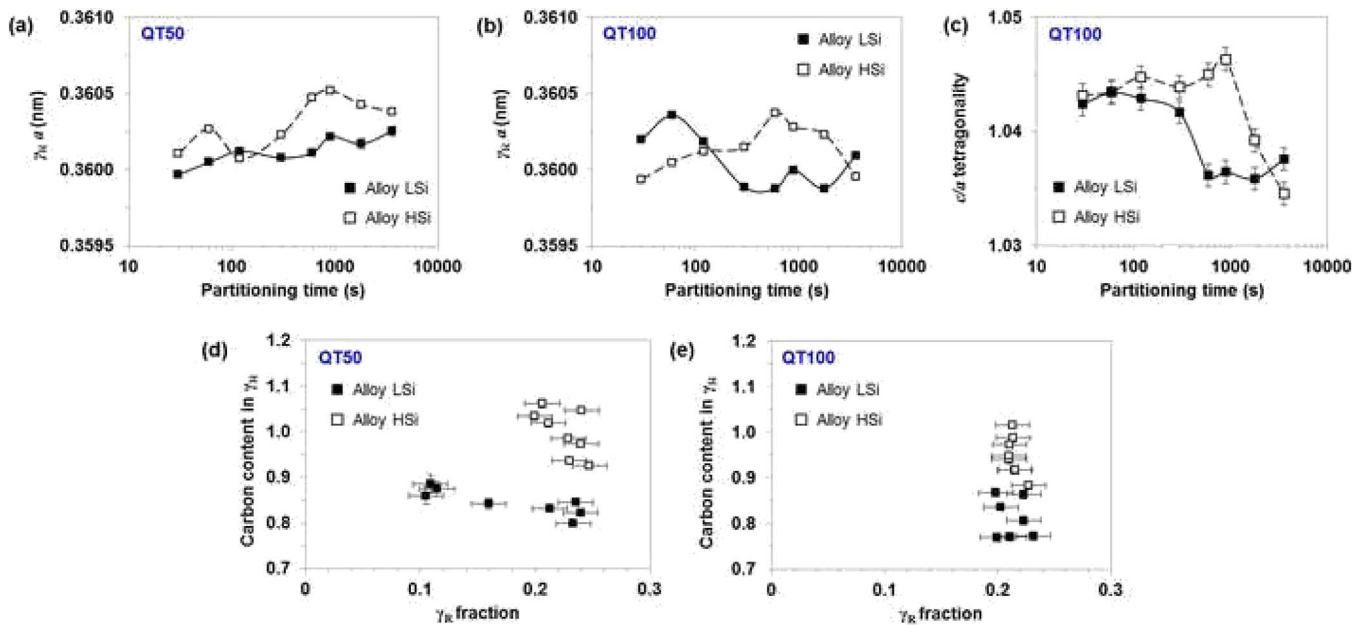
Fig. 6. Lattice parameters of (a) γ_R for QT 50 samples (error bars within markers), (b) γ_R for QT 100 samples (error bars within markers), and (c) c/a ratio of tetragonal α for QT 100 samples. (d) and (e) show plots of γ_R vs. average carbon content in γ_R for samples QT 50 and QT 100, respectively.

summarised in Fig. 5. Fig. 5 (a) and (b) shows the retained austenite fractions for all heat treatments. In most cases, the samples show similar γ_R fractions as in direct quench, except after the QT 50 treatment for alloy LSi, for which from 300 s partitioning, γ_R decreases until it stabilises at 10 %. Panels (c) and (d) in Fig. 5 show the fraction of cubic and tetragonal α, respectively.

Although the fraction of retained austenite does not appear to vary much for increasing partitioning times, it is remarked that the ratio of cubic to tetragonal ferrite evolves, as observed in Fig. 5 (c) and (d). From Fig. 5 (c) it is estimated that when quenching to 100 °C, the M_1 fraction is around 40 % and 60 % for alloys LSi and HSi, respectively. In the case of alloy LSi, the cubic ferrite fraction starts increasing after 600 s of partitioning, whereas in alloy HSi, this appears to occur from 1800 s. The fact that the fraction of cubic α increases with prolonged partitioning indicates the decomposition of austenite. In alloy LSi the reduction in γ_R fraction is seen to occur after 900 s of partitioning, while this is delayed to 3600 s partitioning in alloy HSi. Consistent with the findings in [11], the addition of silicon enhances austenite stability during the partitioning stage, where the decomposition process is delayed for the silicon-containing alloy. It is also remarked that according to the results for QT 100, the fraction of γ_R remains the same regardless of the partitioning stage, and that the only difference is in the proportion of the cubic and tetragonal ferrite.

The room temperature measurement of the γ_R lattice parameters are summarised in Fig. 6 (a) and (b), and the tetragonality (c/a ratio) of M_2

is shown in Fig. 6 (c). The carbon content in γ_R can be related to the lattice parameter by the following empirical formula:

$$a(\gamma_R)[\text{nm}] = 3.572 + 0.00033w_C + 0.00012w_{Mn} - 0.000157w_{Si} + 0.00056w_{Al}. \tag{2}$$

Eq. (2) is obtained from the empirical formula used by Seol et al. [16], where w_i is the concentration of the alloying element i (wt %). When using Eq. (2), an assumption is made that no partitioning of substitutional elements occur during the isothermal holding at 200 °C, where their diffusivity would be limited. APT results in Figs. 9 and 10 confirm this by a constant concentration of substitutional alloying elements across the M_1 and retained austenite interface.

The plots in panels (d) and (e) in Fig. 6 represent γ_R vs. carbon content in γ_R extracted using Eq. (2). In the QT 50 samples, it is seen that as austenite fraction decreases, the average carbon content in γ_R shows a tendency to increase. This is similar to the observations made by van Dijk et al. [17]. The observed trend is interpreted in the following way. Based on the dilatometer and XRD results, there is evidence that austenite decomposition occurs at some point during the partitioning stage. This implies that while some local regions of austenite become carbon-enriched due to the partitioning process from M_1 to γ, the regions where the carbon concentration is relatively low will decompose into bainitic ferrite. With longer partitioning time, only the austenite regions where the local carbon concentration is high enough to resist the $\gamma \rightarrow \alpha$ transformation will remain.
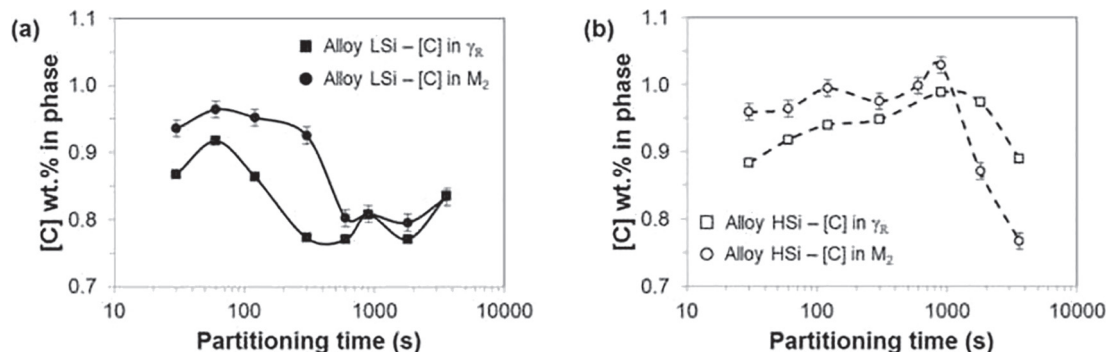

Fig. 7. Calculated carbon content, [C], in retained austenite and M_2 based on the lattice parameters measured by XRD for the samples QT100 for (a) alloy LSi and (b) alloy HSi.
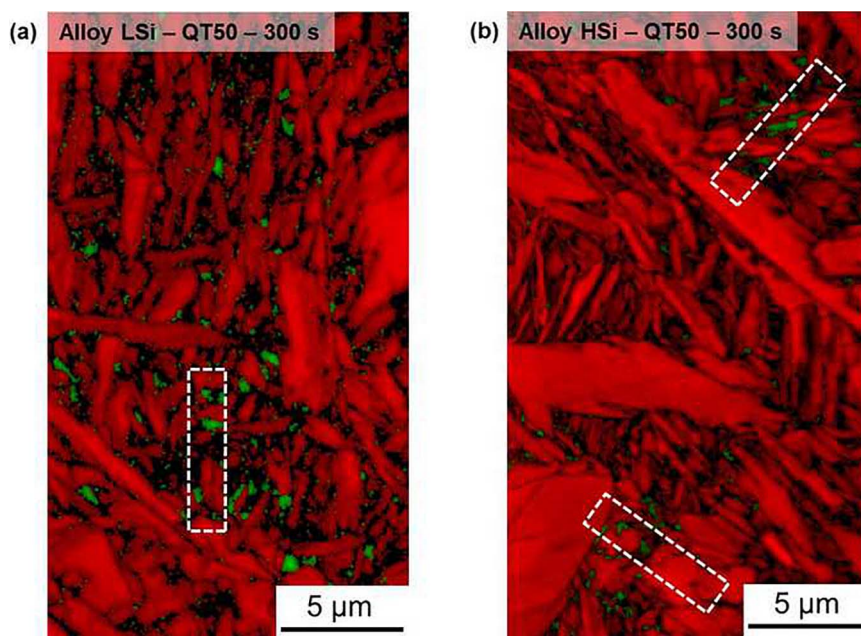
Fig. 8. Combined image quality (IQ) and phase (P) maps obtained from EBSD maps in samples (a) alloy LSi and (b) alloy HSi, where the colours red and green indicate ferrite and austenite, respectively, and the black pixels represent unindexed data points (confidence index below 0.1). The white rectangles show the regions of interest selected for the lift out procedure. (For interpretation of the references to colour in this figure legend, the reader is referred to the web version of this article.)

Furthermore, the slope for alloy HSi is steeper than that of alloy LSi, hinting to a higher degree of carbon enrichment in austenite during partitioning. However, in the case of the QT 100 samples, no significant trend can be seen. This can be explained by considering the formation of M_2, at the end of the cycle. It is reported in the literature that the martensitic transformation induces a compressive hydrostatic strain on the austenite grains [17–19]. Therefore, the formation of fresh martensite during the final cooling will affect the quantification of carbon content in γ_R. This is corroborated in Fig. 7. The average carbon contents in γ_R and M_2 are represented on the same graph. It is observed that for both alloys, the average carbon content appears to be higher in M_2 than in γ_R, except after long partitioning time for alloy HSi. This is counterintuitive, since during the final cooling, the stable austenite is expected to be more enriched in carbon. Therefore, the actual carbon content in γ_R is most likely underestimated due to compressive strains within the retained austenite.

Expanding on the transformation strain discussion, it was recently proposed by Nakada et al. [19] that the presence of the hydrostatic strain in the untransformed austenite provides a stabilising effect on the austenite. In Fig. 2 (c) in Section 3.1, it was observed that with lower quenching temperatures, austenite remains stable to lower temperatures during the second quench. It was previously described that this could be due to the carbon stabilising the austenite during the partitioning stage. However, in light of the discussion regarding the compressive transformation strain, it is also possible that an additional austenite stabilising effect is taking place. As the QT is lowered, higher fractions of martensite are to be expected. This would also increase the transformation strain, hence stabilising the austenite to lower temperatures.

3.3. Atom probe tomography

Atom probe tomography (APT) measurements were carried out in order to observe carbon redistribution across the M_1/γ_R interface, and within the bulk of M_1 and γ_R. The chosen condition was QT 50 for both alloys, partitioned at 200 °C for 300 s, as no M_2 is observed at room temperature. In order to locate the austenite grains in the microstructure, EBSD was carried out. The EBSD maps containing image quality and phase information are shown in Fig. 8 (a) and (b). The selected

regions of interest are marked on the EBSD maps, where regions rich in austenite were selected to maximise chances of observing austenite regions. Eight tips were extracted from alloy LSi, and ten tips were extracted from alloy HSi. Although initially, at room temperature, the microstructure consists of M_1 and γ_R, it is highly likely that the latter transforms into martensite inside the analysis chamber (at 20 K). Nevertheless, given the restricted diffusivity of carbon at such low temperature, no further carbon redistribution is assumed to have occurred at 20 K.

Figs. 9 and 10 show representative images of the tip reconstructions. The tips were systematically analysed as follows: a cylindrical region of interest of diameter 15 nm and length that spans along the entire tip was defined, from where a 1D concentration profile of the alloying elements carbon, silicon and manganese were extracted. The red features shown in the figures correspond to 1 at.% (~ 0.2 wt%) carbon isosurface, which indicate carbon-depleted regions considering that the bulk carbon content in the alloys is of 4.4–4.5 at.% carbon (~ 1 wt%).

As seen from Figs. 9 and 10, there appear to be two sections where different carbon redistribution is observed. The criterion used for distinguishing M_1 and γ_R is based on the carbon profile. The γ_R is expected to have a carbon content close to the original carbon content of the alloy, i.e. 4.4–4.5 at.% carbon in the grain centre. In the case of M_1, carbon depletion is expected since XRD results do not show signs of tetragonality in the ferrite peaks in samples QT50. Furthermore, in dilatometry, a large contraction is observed in the beginning of the partitioning stage that would be consistent with a decrease in the atomic volume in tetragonal martensite as it becomes depleted in carbon.

Having located the approximate position of the interface, a second region of interest is defined, in the form of a cylinder of diameter 15 nm and 100 nm length. Great care was taken in order to ensure that the analysis region was perpendicular to the studied interface. The location of the analysis region and the 1D concentration profile across the 100 nm length are shown in the insets labelled (b), (d) and (f). The location of the M_1/γ_R interface within the analysis volume was estimated in the following way. The 1 at.% carbon isosurface region is considered to be M_1, which due to tempering, is composed of a carbon-depleted matrix and carbon-rich regions that indicate the presence of carbides. Then, the intersecting region between the cylinder and the 1 at.% carbon
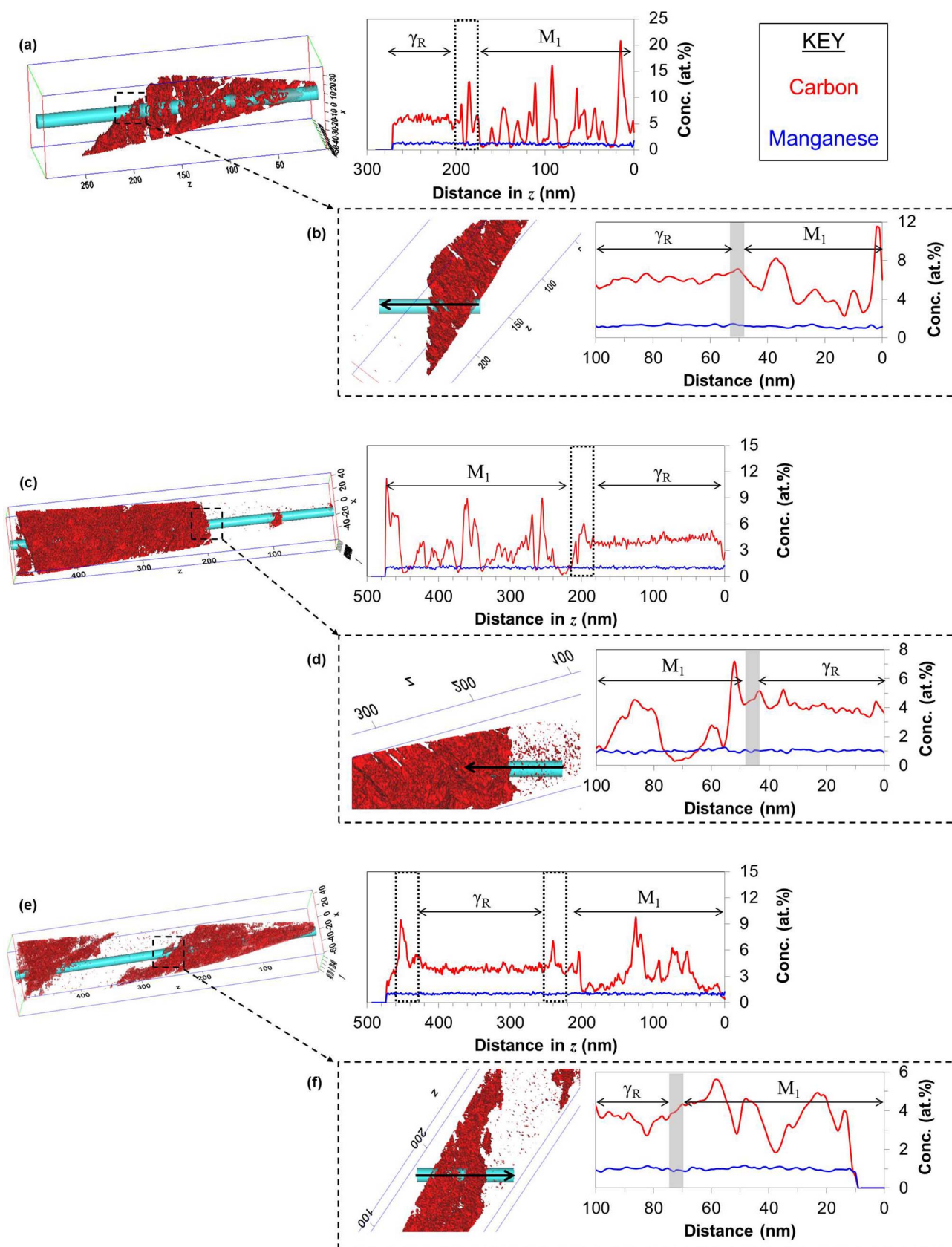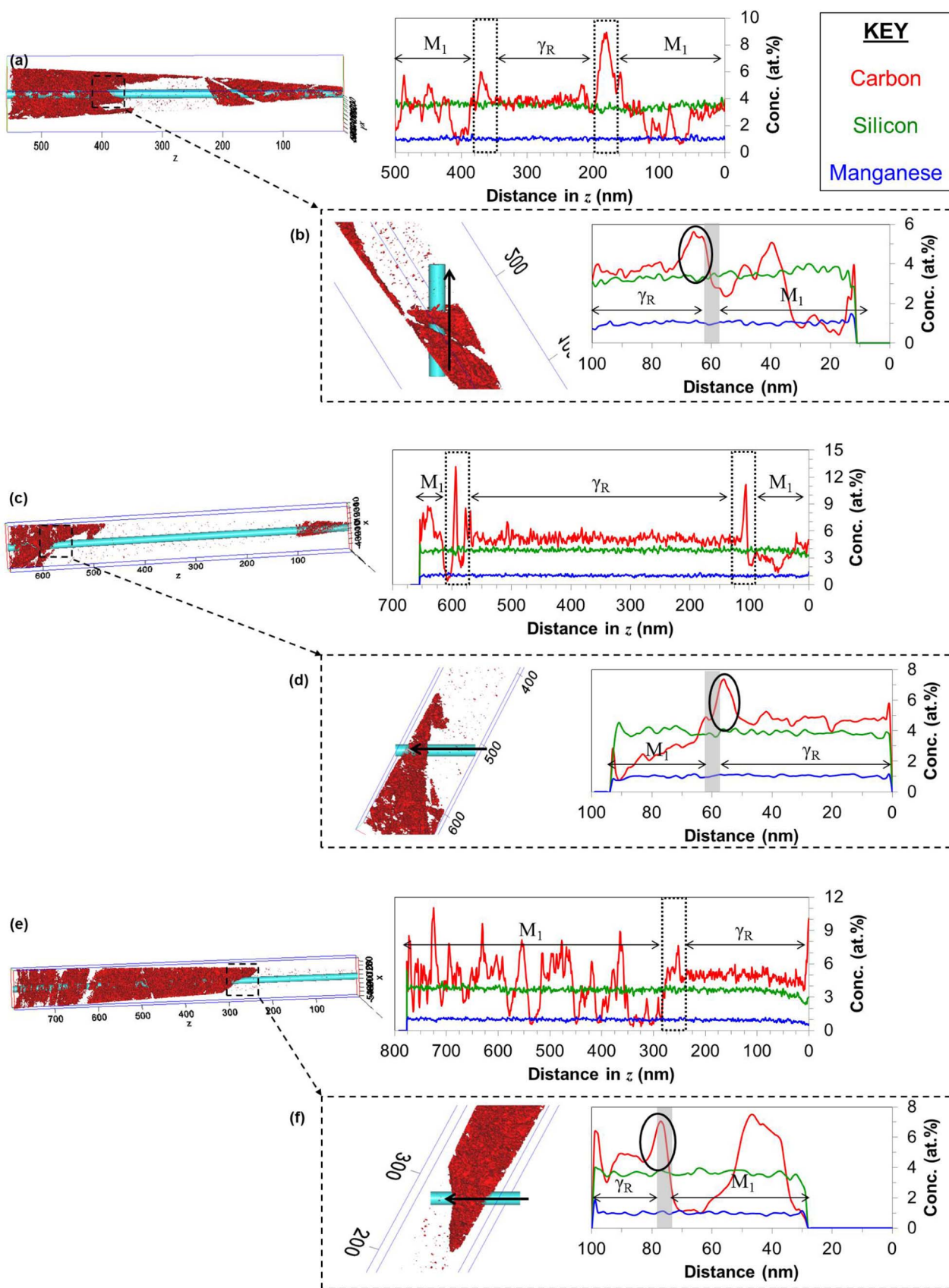
Fig. 9. (a), (c) and (e) show reconstructions of three different tips extracted from alloy LSi, for the sample that has been quenched to 50 °C and partitioned for 300 s at 200 °C. Labelled regions are shown of γ_R and M_1. Carbon isosurfaces of 1 at.% (~ 0.2 wt%) represent carbon-depleted M_1 regions. Figures (b), (d) and (e) show a magnified view of the respective interface region, where the grey region shows the location of the interface. (For interpretation of the references to colour in this figure legend, the reader is referred to the web version of this article.)

Fig. 10. (a), (c) and (e) show reconstructions of three different tips extracted from alloy HSi, for the sample that has been quenched to 50 °C and partitioned for 300 s at 200 °C. Labelled regions are shown of γ_R and M_1. Carbon isosurfaces of 1 at.% (~ 0.2 wt%) represent carbon-depleted M_1 regions. Figures (b), (d) and (e) show a magnified view of the respective interface region, where the grey region shows the location of the interface. (For interpretation of the references to colour in this figure legend, the reader is referred to the web version of this article.)
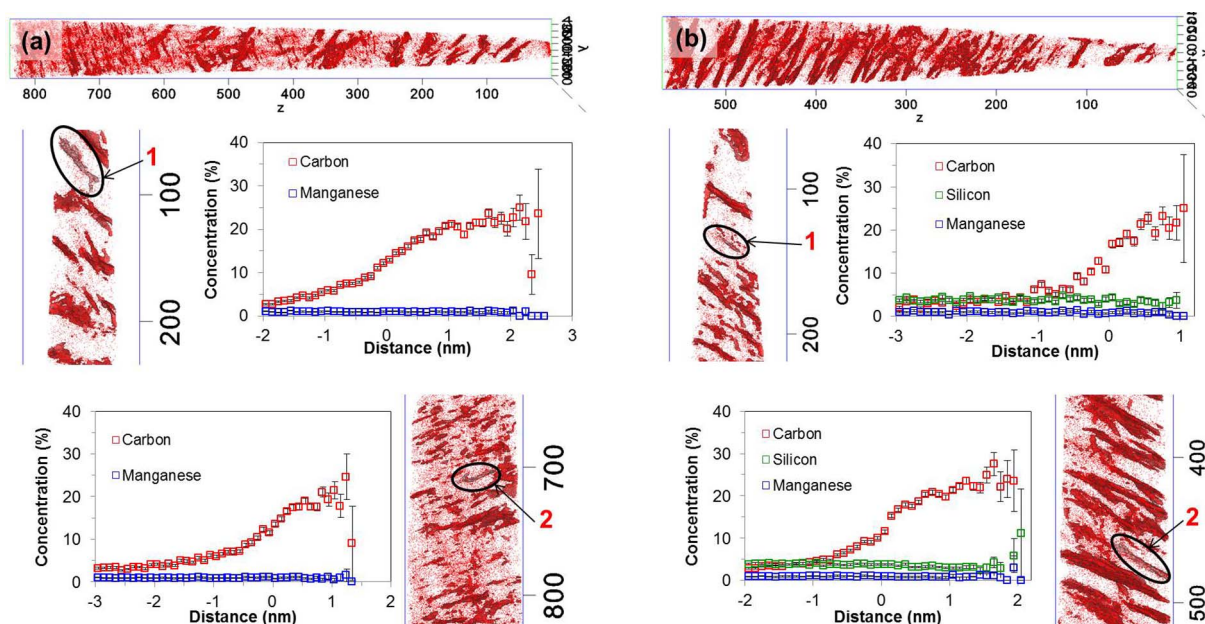
Fig. 11. APT reconstruction of the tempered martensite (M_1) region, for (a) alloy LSi, and (b) alloy HSi, where the red features represent a 12 at.% carbon iso-concentration surface, where the proxigram profile is also shown. (For interpretation of the references to colour in this figure legend, the reader is referred to the web version of this article.)

isosurface is considered to be the interface between M_1 and γ_R. The approximate location of the interface is shaded in grey in Figs. 9 and 10.

It is observed that for alloy LSi, the carbon profile across the interface is relatively smooth. On the other hand, alloy HSi (circled regions in the insets (b), (d) and (f)) shows that the carbon concentration in M_1 rises to 5–7 at.% close to the interface, and drops to 4 at.% as it goes to the interior of the austenite grain. This is consistent with theories proposed in the literature, where the carbon diffusivity in austenite is an important rate-determining factor [20,21]. Due to the sluggish diffusivity of carbon in austenite, a concentration gradient is observed close to the interface.

This particular redistribution of carbon across the M_1/γ_R interface is only observed in alloy HSi. No consistent signs of carbon enrichment across the interface is seen in alloy LSi. The XRD results showed a decrease in the retained austenite fraction from 300 s partitioning in alloy LSi, indicating the decomposition of austenite during the partitioning stage. Therefore, it is seen that in the presence of silicon (alloy HSi) carbon enrichment in austenite takes place, thus stabilising the austenite. Conversely, in the absence of silicon, no carbon partitioning into austenite is observed and decomposition of austenite takes place. It is also worth noting that under such partitioning conditions, i.e. 300 s at 200 °C, no redistribution of manganese nor of silicon is observed by APT.

The M_1 microstructure was further analysed by APT, as shown in Fig. 11. In both alloys, similar results are obtained. The red features represent carbon-rich zones, where by means of the proxigram profile, it shows that they contain $\sim$ 25 at.% carbon. The fact that there is an inhomogeneous distribution of carbon showing a carbon-depleted matrix with carbon-rich features in the tempered martensite, makes it very likely that these features correspond to carbides. Furthermore, it can also be observed that the silicon and the manganese distributions remain homogeneous. This implies that should these carbon-rich features correspond to carbides, the precipitation process occurs under para-equilibrium conditions, where the carbide retains the concentration of the substitutional elements. This is consistent with the findings from the work by Toji et al. [4], where cementite was reported to have formed under para-equilibrium conditions.

From the APT study it is observed that the processes of carbide precipitation and carbon partitioning from martensite into austenite occur simultaneously.

4. Concluding remarks

Two model alloys of composition Fe–1C–1Mn wt% (alloy LSi) and Fe–1C–1Mn–2Si wt% (alloy HSi) were subjected to Q & P style heat treatments in order to understand the influence of silicon in the carbon competing processes and the stability of austenite during the partitioning stage. By means of studying microstructures formed by several experimental heat treatments, the following conclusions are drawn:

1. In the initial stage of partitioning, M_1 becomes depleted in carbon, where carbon readily partitions to the surrounding microstructural constituents.
2. The process of carbide precipitation occurs in both alloys, regardless of silicon content. Furthermore, when precipitation first occurs, no partitioning of the alloying elements is found to have occurred.
3. The addition of silicon stabilises the austenite phase during the partitioning stage, and retards the austenite decomposition process. At the atomic level it is observed that the addition of silicon favours the partitioning of carbon from M_1 into γ, where a built-up of carbon is observed at the edge of the austenite grain.
4. At room temperature, γ_R is strained due to the occurrence of M_2, which affects the lattice parameter measurements by XRD, hence giving an unreliable carbon content estimation.
5. Austenite stabilisation may occur by both carbon enrichment, and by the transformation compressive strain induced by the formation of martensite surrounding the austenite grains.